Asymmetry of acto-myosin cortices as active fluids shape cells in organoids

Tristan Guyomar,[1,2,3,4] Linjie Lu,[1,2,3,4] Tetsuya Hiraiwa,[5,6,7,*] and Daniel Riveline[1,2,3,4,†]

[1] *Institut de Génétique et de Biologie Moléculaire et Cellulaire, Illkirch, France*
[2] *Université de Strasbourg, Illkirch, France*
[3] *Centre National de la Recherche Scientifique, UMR7104, Illkirch, France*
[4] *Institut National de la Santé et de la Recherche Médicale, U964, Illkirch, France*
[5] *Universal Biology Institute, Graduate School of Science, The University of Tokyo, Tokyo, Japan*
[6] *Mechanobiology Institute, Singapore, National University of Singapore, Singapore*
[7] *Institute of Physics, Academia Sinica, Taipei, Taiwan*

(Dated: August 14, 2024)

Cell cortex is a thin sheet of actin cytoskeleton spanning cell boundaries with rich out-of-equilibrium dynamics. A theoretical description of the cortex as an active fluid enables to capture cell shapes dynamics in 3D tissues. However models integrated with calibration of parameters and quantitative experiments are lacking so far. Here we report that cells in organoids and in cysts have conserved apico-basal-lateral asymmetric compositions in actin and in myosin, and we quantify their densities and mechanical properties. This allows to calibrate a new model coupling active fluids with a phase field which reproduces the main features of cell shapes. To test our approach, we successfully predict changes in cell shapes by modulating actin polymerisation in experiments and in simulations. Our study shows how active fluid theory integrated with experiments can determine cell shapes in 3D tissues.

Cells and tissues are shaped by the acto-myosin cytoskeleton [1]. This ∼200 nm thin layer represents a gel spanning each cell border. Its dynamics offers rich out-of-equilibrium spatio-temporal patterns during local protrusion [2–5], motility [6–9], or division [10, 11]. Its self-organisation properties have shown their relevance in a variety of conditions *in vitro* [12, 13] and *in vivo* [14–16]. This level of achievement results from a progress in the experimental physics of actin and acto-myosin *in vitro* associated with the development of active fluid physics [17]. Actin gels were shown to promote bead motion through polymerisation *in vitro* [18–20] and acto-myosin gels were reported to undergo contraction [21]. These phenomena were compared to the theory of active gel revisiting the Navier-Stokes equation by adding a new term taking into account the stress generation internally driven by the acto-myosin cortex [17, 21–24]. Progress over the past decades has enabled theoretical predictions and their relevance mainly in single cell often in 2D [10, 25, 26].

However, at this stage, tests of this cytoskeleton/active gel approach are needed in more physiological situations. Cells grow in 3D in *in vivo* environments. Also cell cortex requires specific measurements to evaluate its physical properties in order to associate theoretical parameters with actual fluid characteristics in experiments. These limitations to extrapolate results obtained so far call for new approaches combining control of 3D tissue growth with quantitative experiments allowing to calibrate active fluid based simulations.

In this context, epithelial cysts represent interesting systems. They are composed of cell monolayers surrounding a fluid filled cavity called the *lumen* [27]. Cysts are also reported as the basic structure at the origin of organs [27], ranging from the formation of embryos [28] to the generation of pancreatic ducts for example [29]. With their *in vitro* controls and their relevance for organogenesis with properties shared with organoids (see End Matter), cysts appear as ideal systems to address this interplay between the physics of acto-myosin cortex and its theoretical description with active fluid formalism.

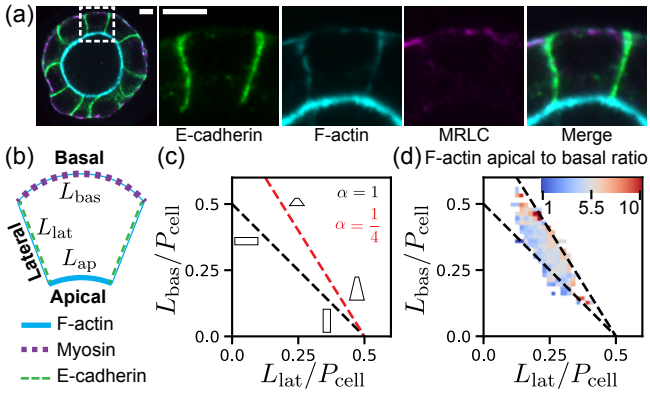

FIG. 1. Correlation between acto-myosin cortical density and cell shape in MDCK cysts. (a) Snapshots of MDCK cysts (2D cut and zoom in) fixed and stained for E-cadherin (green), F-actin (cyan), myosin (magenta). Scale bars, 5 μm. (b) Typical mean cell description used to quantify the relevant geometrical quantities to describe the cell cortex and the cell shape. (c) Schematic description of the cell shape diagram. Oblique lines correspond to different apical to basal length ratios α as described in the main text. Moving along the line changes the aspect ratio of cells w.r.t. the lateral length. (d) F-actin apical to basal intensity ratio correlation with cell shape. $P_{\rm cell}$, cell perimeter. For all measurements, N = 3 experiments, n = 791 cells quantified in 5-day-old MDCK cysts.

In this Letter, we investigated quantitatively the morphological and mechano-chemical features of cells in a 3D

epithelial cyst. We focus on Madin-Darby Canine Kidney (MDCK) epithelial cysts, which allowed us to perform experimental characterizations by quantifying the composition and structures of the gel density and measure its mechanical characteristics (see Materials and Methods in End Matter). We designed in parallel a theory for the active fluid and performed numerical simulations for the cortex coupled to a phase field. We predict how the cortex dynamics determine cell shapes in epithelial cysts. We tested these predictions successfully by changing specifically actin dynamics and obtained predicted shapes.

We first characterised the cell shape with these cysts by acquiring typical images of actin and myosin signals in live and in fixed samples (Fig. 1(a) , SM [36] and Fig. S3(a)). Cysts were invariant by rotation and we could derive a typical cell shape with its actin and its myosin distributions at the cortex in the middle cross-section of each cyst (Fig. 1(a,b), Fig. S3 and Video 1). Strikingly, actin and myosin were asymmetrically distributed around each cell. Actin was thick and enriched in the apical side whereas the myosin layer was thinner and mainly localised at the basal sides (Fig. 1(a) and Fig. S3(e)). The lateral sides were essentially even in actin distributions. We measured that the F-actin intensity was about 5 times higher in the apical cortex than in the basal one and about 7 times higher in the apical cortex than in the lateral one (SM [36], Fig. S3(c), and Table I). We found that the myosin intensity was about 3 times higher in the basal cortex than in the apical one and about 4 times higher in the basal cortex than in the lateral one (Fig. S3(d)). Such anisotropies were conserved in time for MDCK spheroids (Fig. S3(a)) and in several organoids, *i.e.*, in mES epiblast organoids and in pancreas spheres derived from mouse pancreatic progenitor cells [37] (Fig. S1(a) and SM [36]).

Next we quantified and tested potential correlations between cell shapes and the actin and myosin concentration at the cortical layers. We represented the cell shape in a diagram that can capture most of its morphological attributes. We define $L_{\rm ap}$, $L_{\rm bas}$, $L_{\rm lat}$ as respectively the apical, basal and lateral lengths and the total cell perimeter P that we measured on fixed samples (Fig. 1(b) and SM [36]). By construction, $P = L_{\rm ap} + L_{\rm bas} + 2L_{\rm lat}$. By defining the apical length as a fraction of the basal length: $L_{\rm ap} = \alpha L_{\rm bas}$, one can represent $\frac{L_{\rm bas}}{P} = \frac{1}{1+\alpha}\left(1 - 2\frac{L_{\rm lat}}{P}\right)$ (Fig. 1(c)). We used this cell shape representation to look for correlations between cell shape and intensity ratios of actin and myosin, curvatures and lumen occupancy (defined as the ratio of lumen to cyst volumes) (Fig. 1(d), SM [36] and Fig. S1(b) and S4). We noted a strong correlation between F-actin apical to basal ratio and trapezoidal shaped cells (Fig. 1(d)), consistent with the hypothesis that the cortical gel is involved.

Localisation alone was not yet informative about the mechano-chemical parameters of these active gels. To interrogate their characteristics, we used the Fluorescence Recovery After Photobleaching (FRAP) and laser ablation of apical, basal and lateral sides with MDCK cysts cultured from MDCK cell lines stably expressing fluorescent Green Fluorescent Protein (GFP) fused proteins, actin-GFP or myosin regulatory light chain-GFP (MRLC-GFP), see SM [36]). Results are given in Fig. 2, Fig. S5 and in Videos 2-5. FRAP experiments revealed that the mobile fraction of the apical cortex was lower than the basal and lateral ones. The characteristic time of diffusion (orders of seconds, similar to reported values [38, 39]) of G-actin monomers was small compared with the characteristic time associated to transport and assembly of F-actin filaments and network (orders of tens of seconds) (Fig. 2(c,d)). Interestingly, the time of transport was different by a factor of 4 between apical and basal sides, which substantiates again the asymmetry between sides. Finally, we determined that both sides were contractile based on laser ablation experiments and initial recoil velocity, $v_{\rm recoil}^{\rm ini}$, measurements (Fig. 2(e,f)). These experiments allowed to extract mechano-chemical parameters summarized in Table I.

TABLE I. Comparison of the apical-basal-lateral measurements with intensity ratios, FRAP and laser ablation experiments. Ratios of ρ corresponds to ratios of intensities. Measurements are shown as: mean ± standard error of the mean.

Quantities	Apical	Basal	Lateral
$\rho_{\rm apical}^{\text{F-actin}}/\rho_i^{\text{F-actin}}$	1	5.1 ± 0.1	7.1 ± 0.1
$\rho_{\rm basal}^{\rm MRLC}/\rho_i^{\rm MRLC}$	3.2 ± 0.1	1	4.3 ± 0.1
$\tau_{\rm recovery}$ (s)	122 ± 9.2	29.4 ± 4.1	27.3 ± 3.3
$v_{\rm recoil}^{\rm ini}$ (μm.s^{-1})	5.6 ± 0.2	8.4 ± 0.3	8.2 ± 0.6

Next, we theoretically tested our hypothesis that the asymmetry in cortex distribution is a key factor to determine cell shape in a cyst, through numerical simulations based on multicellular phase-field (PF) model [37, 40, 41] coupled to active gel equations [42, 43] (see End Matter).

The geometry of cells is described by PF variables $\phi(\boldsymbol{r}, t)$, defined for each cell, and cortical gel is confined in the interface of cellular PF by the coupling free energy:

$$F_{\rm coupling}[\phi, \rho] = -\int_\Omega f_{\rm coup}\rho|\boldsymbol{\nabla}\phi(\boldsymbol{r})|\delta\left(\phi(\boldsymbol{r}) - \frac{1}{2}\right)\mathrm{d}\boldsymbol{r} \quad (1)$$

with $f_{\rm coup}$ controls the strength of coupling and Ω the simulation domain area. This free energy term adds a new term to the cellular-PF dynamics (see Eq. (S28) of SM [36]). This coupling term induces a global contractility which counteracts the volume control and adhesion energies already set in the cell shape dynamics. $\rho(r, t)$ obeys the conservation equation with the source of cortical gel at the cellular-PF interface:

$$\partial_t\rho + \boldsymbol{\nabla}\cdot(\rho\boldsymbol{v}) = -A_{\rm deg}\rho + A_{\rm gen}|\boldsymbol{\nabla}\phi|\delta(\phi - 1/2)\ , \quad (2)$$

where the first and second terms on the right-hand side are the degeneration and source at the cell interface, re-

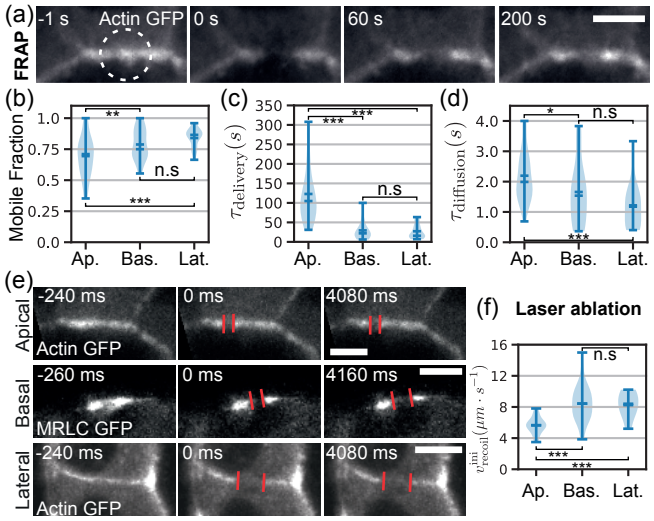

FIG. 2. Quantification of mechano-chemical properties of the acto-myosin gels at different locations of the cell cortex in day 5 MDCK cysts. (a) Snapshots of FRAP experiments performed on the apical cortex of MDCK cysts labelled for actin-GFP (grey) (Video 2). Measurements of (b) mobile fraction, (c) τ_{delivery} and (d) $\tau_{\text{diffusion}}$ at apical, basal and lateral cortices. $N = 3$ experiments, $n = 60$ cells (apical), $n = 30$ cells (basal and lateral). (e) Snapshots of laser ablation of the cortex performed on the apical, basal and lateral cortex of MDCK cysts labelled for actin-GFP (grey) - apical and lateral) or MRLC-GFP (grey - basal) (Videos 3-5). (f) Initial recoil velocity for apical, basal and lateral sides measured from the initial distance created after laser ablation. $N = 4$ experiments, $n = 43$ cells (apical), $n = 45$ cells (basal), $N = 3$ experiments, $n = 8$ cells (lateral). Statistical tests: *: $p < 0.05$, **: $p < 0.01$, ***: $p < 0.001$, n.s: $p > 0.05$. Scale bars : 5 μm.

spectively. A_{deg} and A_{gen} represent the turnover rate and production speed, respectively. $v_\alpha(r,t)$ is the gel velocity field and given by the force balance: $\partial_\beta \sigma_{\alpha\beta} = \gamma v_\alpha$, where $\sigma_{\alpha\beta}$ is the total stress tensor, γ is a friction coefficient and $\alpha, \beta = x, y$. We write the stress tensor as $\sigma_{\alpha\beta} = \sigma_{\text{viscous}} + \sigma_{\text{active}} = 2\eta v_{\alpha\beta} - \Pi_{\alpha\beta}(\rho)$ with the velocity gradient tensor $v_{\alpha\beta} = (\partial_\alpha v_\beta + \partial_\beta v_\alpha)/2$ and choose to follow Ref.[42] to express Π in terms of the gel density ρ with $\pi_{\alpha\beta}(\rho) = -a_{\alpha\beta}\rho^3 + b_{\alpha\beta}\rho^4$. For $a > 0$, the active gel is contractile whereas, for $a < 0$, the active gel is extensile [44].

We performed the numerical simulations based on the equations presented above (SM [36]). Taking advantage of the phase field formulation of the model, we defined apical, lateral and basal cortices and imposed different parameters to each of them (SM [36] for the complete set of parameters values). We modeled a 2D cut of a cyst composed of 6 cells, and we depicted the main results in Fig. 3 and in Video 6. We first tested how a change in uniform surface tension would impact the cell and cyst shapes by adding no additional active stresses but setting various uniform turnover dynamics in the cell cortices (Fig. 3(a) and SM [36]). As the turnover rate increases, so does the active gel density ρ and the cells became rounder. Using similar diagrams as introduced in Fig. 1(c), we quantified these shape changes (Fig. 3(b)) and we observed that for a given set of parameters (lumen pressure, cell-cell adhesion, ECM elasticity, total cell number) the morphology of cells evolved mainly on a straight line in the cell shape diagram as A_{gen} varies.

Next, we implemented asymmetric turnover rates between apical, lateral and basal cortices (Fig. S8 and SM [36]). Interestingly, asymmetries in the turnover rate distributions yielded a variety of cyst morphologies (Fig. S8(a)), richer than the symmetric case (Fig. 3(a)). This was further illustrated in the cell shape diagram (Supp. Fig. S8(b)) where asymmetric turnover rates led to departure from the previously highlighted trajectories (Fig. 3(a)). We then changed the physical origin of stress generation, by testing how the asymmetry of the nature of active stresses would impact cell shapes in cysts. We kept symmetric turnover rates and we tuned the extensile/contractile nature of apical and basal cortices (Fig. 3(c)). Strikingkly, whereas the active gel density remained constant, the asymmetric nature of stresses alone led to large changes in shapes. For example, in the case of apical contractile and basal extensile (Fig. 3(c,d), green point), the extensility of the basal active gel yielded less active stress and more tangentially elongated cells. Finally, we could reproduce MDCK cell phenotypes (Fig. 3(e) and Fig. 1(a) top) when setting asymmetric turnover rates and asymmetric active stresses (SM [36]) following the measurements presented in Fig. 1 , Fig. 2 and recapitulated in Table I .

To test predictions associated to changes in the dynamics of the gel parameters (SM [36]), we altered specifically the polymerisation of actin. Upon incubation with the depolymerising agent latrunculin A (LatA) (M&M), we recorded changes in cell shape and the associated modifications in the actin cortical composition (Fig. 4(a), Fig. S6 and Video 7). We also performed the opposite experiment by incubating cysts with the actin polymerisation enhancer C8BPA [35] (Fig. 4(d) and Video 9). Quantifications are shown in Fig. 4(a-d) and in SM [36]. Strikingly, we could obtain shapes predicted by the associated changes in actin polymerisation in the simulation (variation of A_{gen} in Fig. 4 (e,f) and Video 10).

We have shown that asymmetry of the cortex is sufficient to describe cell shapes in cysts and in organoids. We used the physics of active fluids and quantification of the cortex to predict experimental and simulated cell shapes in cysts. This framework could serve as a generic approach to design 3D tissues with molecular strategies and mesoscopic consequences on cell and cyst shapes.

We report that actin is primarily present in the apical side whereas acto-myosin is assembled at the basal side. One could have thought that actin gel would be extensile and acto-myosin gel contractile, like in former

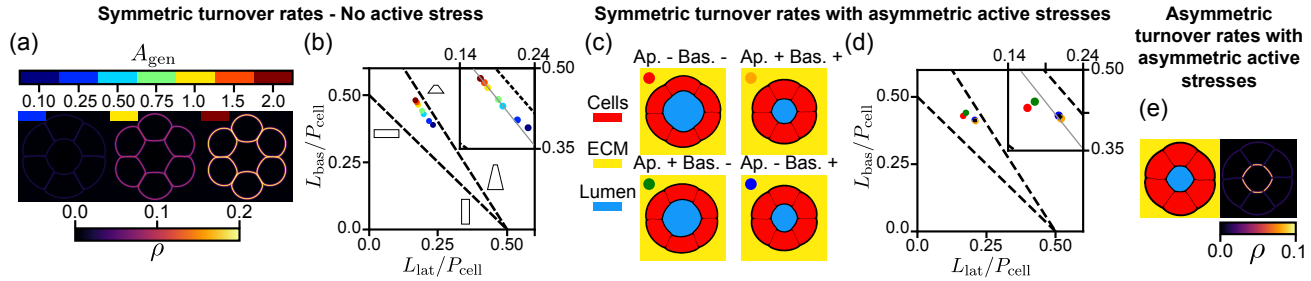

FIG. 3. Asymmetry in active fluid cortices generates relevant cell shapes in numerical simulations. (a) Snapshots of simulated 2D cuts of cysts with symmetric apical, basal and lateral turnover rates at steady state for different turnover rate magnitudes, active gel density ρ is represented (Video 6). (b) Cell shape evolution when $A_{\rm gen}$ is modified globally. (c) Snapshots of simulated 2D cuts of cysts with symmetric turnover rates but asymmetric additional extensile/contractile active stresses. Cells (red), lumen (blue) and an elastic ECM (yellow) are represented. All simulations started from the same initial condition and were stopped after 300000 steps. (d) Cell shape changes associated with asymmetry in active stresses. Same symbols in (c) and (d). (e) In the case of asymmetric turnover rates, parameters were chosen to match the experimental data presented in Table I.

studies [18, 45, 46]. This asymmetry in composition does not translate into extensile and contractile gels respectively. Rather they are both contractile and this suggests that another mechanical asymmetry is at play. This also illustrates that the molecular knowledge of the gel composition is not sufficient to explain the mechanics and shape of the cortex.

Our description integrates generic cellular properties and should be broadly applicable in other organoids and in 3D tissues. It will be interesting to interrogate the cortical properties in each case to identify conservations and differences between systems.

END MATTER

Cysts in organoids - Cysts also emerge in *organoids* which are three-dimensional organ-models formed *in vitro* from stem cells when cultured in the relevant environments [30]. Interestingly, differentiated epithelial cells can also mimic cell shape dynamics observed in organoids. Indeed, they often share common cortical proteins as well as adhesion complexes across systems. These shared points allow to probe and establish phenomena with reliable extrapolation to organs found *in vivo*. Altogether the integrated comparisons and characterisation of epithelial cysts and organoids with active gels simulations appear as a powerful route to implement and test active fluid descriptions for cell shapes determination in 3D tissues. Quantitative measurement of each cell shape and mechano-chemical characterization of cells in a cyst are lacking so far.

Materials and Methods - Briefly, mouse embryonic stem cells (mES) epiblasts and pancreas spheres were prepared according to protocols of Refs. [31] and [32], respectively. MDCK II cell lines - wild type and expressing fluorescent markers - were cultured using Minimum Essential Media (MEM) supplemented with 5% Fetal Bovine Serum (FBS). We obtained MDCK cysts lying within the same focal plane using a protocol adapted from Refs. [33, 34]. Coverslips were activated by O_2 plasma and coated with a 100% Matrigel solution (Corning BV: 356231). Single cells were deposited at a density of 15,000 cells/cm^2 covered next by another layer of 10 μl 100% Matrigel. To investigate the role of actin polymerisation, we used 200 nM of inhibitor latrunculin A (Sigma Aldrich #L5163) and 100 μM of C8N6 BPA polyamine (C8BPA) activator of actin polymerisation [35]. Images were acquired with a Leica DMi8 confocal microscope equipped with a Yokogawa CSU W1 spinning disk and with an OrcaFlash 4.0 camera for the Fluorescence Recovery After Photobleaching (FRAP). Laser ablations of the acto-myosin cortex were performed using the FRAP module from a Leica SP-5 inverted microscope (see SM [36] for more details in immunofluorescence and in analysis).

Phase Field (PF) modeling - We simplified cysts into three components: cells, lumen and ECM. Their geometries are described by using PF variables $\phi_i(\boldsymbol{r},t)$ ($i = 1, ..., m$; one for each cell), $\ell(\boldsymbol{r},t)$ and $e(\boldsymbol{r},t)$, respectively. The regions where each PF variable takes 1 and 0 represent the inside and outside of the corresponding phase, respectively. We defined for each cell a cortical gel confined in the vicinity of the cellular interface, set by $\phi_i(r) = 1/2$, which is modeled as an active gel of density field $\rho_i(\boldsymbol{r},t)$ obeying the 2D extension of the 1D model developed in Refs. [42, 43]. Dynamics of the field variables is given in SM [36]. Each PF variable obeys mainly the standard multicellular PF model [37, 40, 41], under the assumptions: (i) all cells have identical optimum cell size, cell-cell adhesion, cell-ECM adhesion and excluded volume; (ii) dynamics of lumen volume are driven by osmotic pressure differences; and (iii) the ECM is described as an elastic material.

Detailed comparisons for changes in actin dynamics - To test predictions associated to changes in

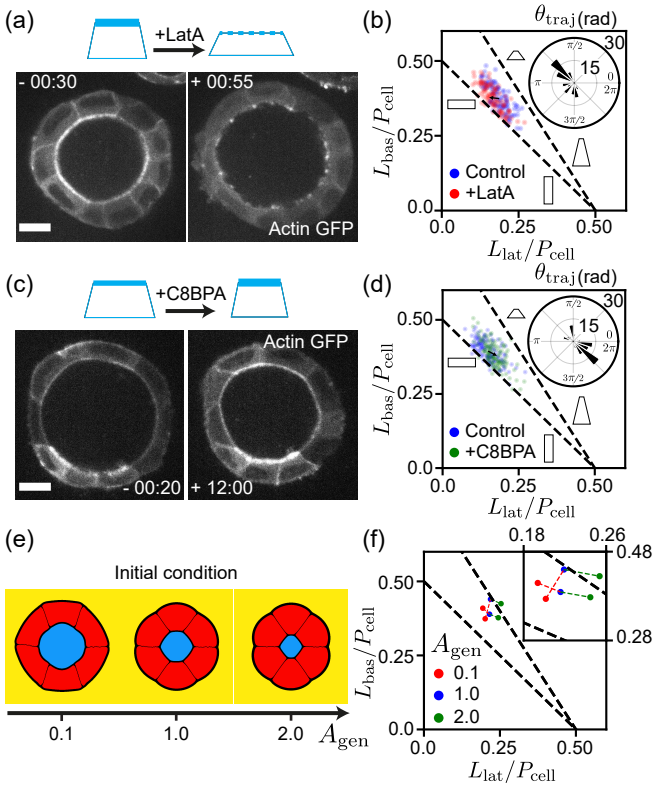

FIG. 4. Specific modifications of actin polymerisation lead to shapes predicted by the active fluid numerical simulations. (a) Inhibition of actin polymerisation by incubating MDCK cysts with LatA. Snapshots of an individual cell before and after treatment (Video 7). (b) Cell shape diagram showing the effect of LatA on cells: cells tend to become flatter and elongate longitudinally. Black arrow represents the motion of the center of mass of the experimental cloud points before and after LatA treatment. N = 3 experiments - n = 97 cells. (c) Enhancement of actin polymerisation by incubating MDCK cysts with C8BPA. Snapshots of an individual cell before and after treatment (Video 9). (d) Cell shape diagram showing the effect of C8BPA on cells: cells tend to become more radially elongated. Black arrow represents the motion of the center of mass of the experimental cloud points before and after C8BPA treatment. N = 3 experiments - n = 117 cells. Insets of (b) and (d): distribution of θ_{traj}, the angle of each trajectory vector in the cell shape diagram corresponding to Lat A or C8BPA treatment respectively. (e) Snapshots of simulated cysts with asymmetric turnover rates but with various baseline polymerisation rates A_{gen} (Video 10). (f) Cell shape diagram showing the effect of enhancing or diminishing active gel polymerisation in simulated cells. Insets of (b) and (d) show that distributions go in opposite directions consistently with insets of (f). Scale bars: 10 μm.

the dynamics of the gel parameters (SM [36]), we altered specifically the polymerisation of actin. Upon incubation with the depolymerising agent latrunculin A (LatA) (M&M), we recorded changes in cell shape and the associated modifications in the actin cortical composition. After treatment, cells became flatter, apical cortices bent away from the lumen and the apical actin gel depolymerised (Fig. 4(a), Fig. S6 and Video 7). After washout, actin cortices were rebuilt and cell shape came back to their configuration prior drug treatment in about 10 hours (Fig. S7 and Video 8). We also performed the opposite experiment by incubating cysts with the actin polymerisation enhancer C8BPA [35]. Actin gels polymerised following the drug incubation and cells became more cuboidal with a tendency of the apical cortex to adopt a positive curvature w.r.t. the cell center of mass (Fig. 4(d) and Video 9). Quantifications are shown in Fig. 4(a-d) and in SM [36]. Strikingly, we could obtain shapes predicted by the associated changes in actin polymerisation in the simulation (variation of A_{gen} in Fig. 4 (e,f) and Video 10). This successful comparison shows that our cortex model can capture the cell shapes and changes its shapes with specific changes in mechano-chemical parameters.

Mesoscopic approach and cytoskeleton organisation - This mesoscopic approach goes also with structural simplifications which may contribute to setting the contractile nature of these cortices. For example, the apical side is composed of villi with folded structures and anchors to the membrane [1]. Orientations of actin filaments are reported to be specific at this level [1]. Our results show that our mesoscopic approach is still successful to explain cell shapes beyond molecular compositions and architecture.

ACKNOWLEDGEMENTS

We acknowledge Kana Fuji and Sakurako Tanida for supporting us to implement numerical simulations. We thank the Riveline group for help and discussions and Erwan Grandgirard and the Imaging Platform of IGBMC. We also thank Anne Grapin-Botton, Masaki Sano and Alf Honigmann and their respective teams for advices and discussions. We thank Makiko Nonomura, Jacques Prost and Karsten Kruse for fruitful discussions. L.L. and T.G. are supported by HFSP and by the University of Strasbourg, and by la Fondation pour la Recherche Médicale (T.G.). T.H. is supported by Seed Fund of Mechanobiology Institute. D.R. acknowledges the Interdisciplinary Thematic Institute IMCBio, part of the ITI 2021-2028 program of the University of Strasbourg, CNRS and Inserm, which was supported by IdEx Unistra (ANR-10-IDEX-0002), and by SFRI-STRAT'US project (ANR 20-SFRI-0012) and EUR IMCBio (ANR-17-EURE-0023) under the framework of the French Investments for the Future Program. D.R. acknowledges the Research Grant from Human Frontier Science Program (Ref.-No: RGP0050/2018).

* thiraiwa@gate.sinica.edu.tw
† riveline@unistra.fr

[1] B. Alberts, A. Johnson, J. Lewis, M. Raff, K. Roberts, and P. Walter, *Molecular biology of the cell*, 6th ed. (Garland Science, New York, NY, 2015).
[2] A. J. Ridley and A. Hall, Cell **70**, 389 (1992).
[3] T. P. Stossel, Science **260**, 1086 (1993).
[4] T. M. Svitkina and G. G. Borisy, The Journal of Cell Biology **145**, 1009 (1999).
[5] T. Svitkina, Cold Spring Harbor Perspectives in Biology **10**, a018267 (2018).
[6] A. B. Verkhovsky, T. M. Svitkina, and G. G. Borisy, Current Biology **9**, 11 (1999).
[7] L. Blanchoin, R. Boujemaa-Paterski, C. Sykes, and J. Plastino, Physiological Reviews **94**, 235 (2014).
[8] D. Caballero, R. Voituriez, and D. Riveline, Biophysical Journal **107**, 34 (2014).
[9] S. L. Vecchio, R. Thiagarajan, D. Caballero, V. Vigon, L. Navoret, R. Voituriez, and D. Riveline, Cell Systems **10**, 535 (2020).
[10] H. Turlier, B. Audoly, J. Prost, and J.-F. Joanny, Biophysical Journal **106**, 114 (2014).
[11] V. Wollrab, R. Thiagarajan, A. Wald, K. Kruse, and D. Riveline, Nature Communications **7** (2016), 10.1038/ncomms11860.
[12] E. Paluch, J. van der Gucht, J.-F. Joanny, and C. Sykes, Biophysical Journal **91**, 3113 (2006).
[13] A.-C. Reymann, J.-L. Martiel, T. Cambier, L. Blanchoin, R. Boujemaa-Paterski, and M. Théry, Nature Materials **9**, 827 (2010).
[14] H. Blaser, M. Reichman-Fried, I. Castanon, K. Dumstrei, F. Marlow, K. Kawakami, L. Solnica-Krezel, C.-P. Heisenberg, and E. Raz, Developmental Cell **11**, 613 (2006).
[15] A. C. Martin, M. Kaschube, and E. F. Wieschaus, Nature **457**, 495 (2008).
[16] C. Bertet, L. Sulak, and T. Lecuit, Nature **429**, 667 (2004).
[17] J. Prost, F. Jülicher, and J.-F. Joanny, Nature Physics **11**, 111 (2015).
[18] T. P. Loisel, R. Boujemaa, D. Pantaloni, and M.-F. Carlier, Nature **401**, 613 (1999).
[19] V. Noireaux, R. Golsteyn, E. Friederich, J. Prost, C. Antony, D. Louvard, and C. Sykes, Biophysical Journal **78**, 1643 (2000).
[20] S. Wiesner, E. Helfer, D. Didry, G. Ducouret, F. Lafuma, M.-F. Carlier, and D. Pantaloni, The Journal of Cell Biology **160**, 387 (2003).
[21] K. Kruse and F. Jülicher, Physical Review Letters **85**, 1778 (2000).
[22] K. Kruse, J. F. Joanny, F. Jülicher, J. Prost, and K. Sekimoto, Physical Review Letters **92**, 078101 (2004).
[23] K. Kruse, J. F. Joanny, F. Jülicher, J. Prost, and K. Sekimoto, The European Physical Journal E **16**, 5 (2005).
[24] M. C. Marchetti, J. F. Joanny, S. Ramaswamy, T. B. Liverpool, J. Prost, M. Rao, and R. A. Simha, Reviews of Modern Physics **85**, 1143 (2013).
[25] F. Julicher, K. Kruse, J. Prost, and J.-F. Joanny, Physics Reports **449**, 3 (2007).
[26] M. Mayer, M. Depken, J. S. Bois, F. Jülicher, and S. W. Grill, Nature **467**, 617 (2010).
[27] S. Sigurbjörnsdóttir, R. Mathew, and M. Leptin, Nature Reviews Molecular Cell Biology **15**, 665 (2014).
[28] S. E. Harrison, B. Sozen, N. Christodoulou, C. Kyprianou, and M. Zernicka-Goetz, Science **356** (2017), 10.1126/science.aal1810.
[29] P. A. Seymour and M. Sander, Diabetes **60**, 364 (2011).
[30] K. Kretzschmar and H. Clevers, Developmental Cell **38**, 590 (2016).
[31] C. Martin-Lemaitre, Y. Alcheikh, R. Naumann, and A. Honigmann, biorXiv (2020), 10.1101/2020.03.13.990135.
[32] C. Greggio, F. D. Franceschi, M. Figueiredo-Larsen, S. Gobaa, A. Ranga, H. Semb, M. Lutolf, and A. Grapin-Botton, Development **140**, 4452 (2013).
[33] A. Chin, K. Worley, P. Ray, G. Kaur, J. Fan, and L. Wan, Proceedings of the National Academy of Sciences **115**, 12188 (2018).
[34] L. Lu, T. Guyomar, Q. Vagne, R. Berthoz, A. Torres-Sánchez, M. Lieb, C. Martin-Lemaitre, K. van Unen, A. Honigmann, O. Pertz, G. Salbreux, and D. Riveline, Nature Physics (2024), 10.1038/s41567-024-02460-w.
[35] I. Nedeva, G. Koripelly, D. Caballero, L. Chièze, B. Guichard, B. Romain, E. Pencreach, J.-M. Lehn, M.-F. Carlier, and D. Riveline, Nature Communications **4** (2013).
[36] Supplementary material is available at ....com, for experimental details, data, experimental videos and a Github repository containing the computer code used in this paper..
[37] L. Lu, K. Fuji, T. Guyomar, M. Lieb, S. Tanida, M. Nonomura, T. Hiraiwa, Y. Alcheikh, S. Yennek, H. Petzold, C. Martin-Lemaitre, A. Grapin-Botton, A. Honigmann, M. Sano, and D. Riveline, biorXiv (2024), 10.1101/2024.02.20.581158.
[38] J. McGrath, Y. Tardy, C. Dewey, J. Meister, and J. Hartwig, Biophysical Journal **75**, 2070 (1998).
[39] K. Luby-Phelps, "Cytoarchitecture and physical properties of cytoplasm: Volume, viscosity, diffusion, intracellular surface area," in *Microcompartmentation and Phase Separation in Cytoplasm* (Elsevier, 1999) pp. 189–221.
[40] M. Nonomura, PLoS ONE **7**, e33501 (2012).
[41] M. Akiyama, M. Nonomura, A. Tero, and R. Kobayashi, Physical Biology **16**, 016005 (2018).
[42] J.-F. Joanny, K. Kruse, J. Prost, and S. Ramaswamy, The European Physical Journal E **36** (2013).
[43] N. Levernier and K. Kruse, New Journal of Physics **22**, 013003 (2020).
[44] The choice of the functional Π is not essential as long as it has a non monotonous dependency in the active gel density if the activity of motors is high enough and reflects that the passive osmotic pressure always dominates at large densities.
[45] H. Boukellal, O. Campás, J.-F. Joanny, J. Prost, and C. Sykes, Physical Review E **69**, 061906 (2004).
[46] P. M. Bendix, G. H. Koenderink, D. Cuvelier, Z. Dogic, B. N. Koeleman, W. M. Brieher, C. M. Field, L. Mahadevan, and D. A. Weitz, Biophysical Journal **94**, 3126 (2008).
[47] T. Watanabe, H. Hosoya, and S. Yonemura, Molecular Biology of the Cell **18**, 605 (2007).
[48] C. Klingner, A. V. Cherian, J. Fels, P. M. Diesinger, R. Aufschnaiter, N. Maghelli, T. Keil, G. Beck, I. M. Tolić-Nørrelykke, M. Bathe, and R. Wedlich-Soldner, Journal of Cell Biology **207**, 107 (2014).

[49] J. Schindelin, I. Arganda-Carreras, E. Frise, V. Kaynig, M. Longair, T. Pietzsch, S. Preibisch, C. Rueden, S. Saalfeld, B. Schmid, J.-Y. Tinevez, D. J. White, V. Hartenstein, K. Eliceiri, P. Tomancak, and A. Cardona, Nature Methods **9**, 676 (2012).

[50] I. D. Coope, J. Optim. Theory Appl. **76**, 381–388 (1993).

[51] J. Firmino, J.-Y. Tinevez, and E. Knust, PLoS ONE **8**, e58839 (2013).

[52] S. Dasgupta, K. Gupta, Y. Zhang, V. Viasnoff, and J. Prost, Proceedings of the National Academy of Sciences **115** (2018).

[53] M. Tyska and M. Mooseker, Biophysical Journal **82**, 1869 (2002).

[54] F. Waharte, C. M. Brown, S. Coscoy, E. Coudrier, and F. Amblard, Biophysical Journal **88**, 1467 (2005).

[55] E. Olsson and G. Kreiss, Journal of Computational Physics **210**, 225 (2005).

[56] A. Badillo, Physical Review E **86**, 041603 (2012).

[57] D. Indana, A. Zakharov, Y. Lim, A. R. Dunn, N. Bhutani, V. B. Shenoy, and O. Chaudhuri, biorXiv (2023), 10.1101/2023.04.20.537711.

[58] *PGI Reference Manual* *https://docs.nvidia.com/hpc-sdk/pgi-compilers/20.4/pdf/pgi20ref-x86.pdf* (The Portland Group Inc., 2020).